Interaction potential for aluminum nitride: A molecular dynamics study of mechanical and thermal properties of crystalline and amorphous aluminum nitride

Priya Vashishta,[1,a)] Rajiv K. Kalia,[1] Aiichiro Nakano,[1] José Pedro Rino,[1,2] and Collaboratory for Advanced Computing and Simulations
[1]*Department of Chemical Engineering and Materials Science, Department of Physics and Astronomy, and Department of Computer Science, University of Southern California, Los Angeles, California 90089-0242, USA*
[2]*Departamento de Física, Universidade Federal de São Carlos, São Carlos, SP 13565-905, Brazil*

(Received 19 May 2010; accepted 12 November 2010; published online 7 February 2011)

An effective interatomic interaction potential for AlN is proposed. The potential consists of two-body and three-body covalent interactions. The two-body potential includes steric repulsions due to atomic sizes, Coulomb interactions resulting from charge transfer between atoms, charge-induced dipole-interactions due to the electronic polarizability of ions, and induced dipole–dipole (van der Waals) interactions. The covalent characters of the Al–N–Al and N–Al–N bonds are described by the three-body potential. The proposed three-body interaction potential is a modification of the Stillinger–Weber form proposed to describe Si. Using the molecular dynamics method, the interaction potential is used to study structural, elastic, and dynamical properties of crystalline and amorphous states of AlN for several densities and temperatures. The structural energy for wurtzite (2H) structure has the lowest energy, followed zinc-blende and rock-salt (RS) structures. The pressure for the structural transformation from wurtzite-to-RS from the common tangent is found to be 24 GPa. For AlN in the wurtzite phase, our computed elastic constants (C_{11}, C_{12}, C_{13}, C_{33}, C_{44}, and C_{66}), melting temperature, vibrational density-of-states, and specific heat agree well with the experiments. Predictions are made for the elastic constant as a function of density for the crystalline and amorphous phase. Structural correlations, such as pair distribution function and neutron and x-ray static structure factors are calculated for the amorphous and liquid state. © *2011 American Institute of Physics*. [doi:10.1063/1.3525983]

I. INTRODUCTION

Though aluminum nitride (AlN) was discovered and synthesized at the end of the 19th century, its technological importance was recognized only in 1980s. Aluminum nitride is a large band gap (6.3 eV) semiconductor. Among electrically insulating ceramic materials, only AlN and beryllium oxide have high thermal conductivity. Aluminum nitride, in particular, is nontoxic, has only one crystal structure (wurtzite), and at atmospheric pressure it dissociates above 2780 K. Aluminum nitride also shows low thermal expansion coefficient and large hardness.

These characteristics make AlN an ideal substrate material for microelectronics, and accordingly extensive theoretical and experimental studies of its properties have been performed. For example, thermodynamic properties, in the range of 5–2700 K, have been reported by Koshchenko *et al.*[1] Ueno and collaborators[2] used x-ray diffraction to study the structural phase transition under high pressure up to 30 GPa. Energy-dispersive x-ray diffraction using a synchrotron x-ray source was used by Xia *et al.*[3] at pressure up to 65 GPa to observe a structural transformation to the rock-salt phase. Meng *et al.*[4] determined the elastic constants in sputter deposited AlN thin film on Si (111). More recently, Uehara *et al.*[5] used x-ray diffraction to determine the equation of states of the rock-salt phase up to 132 GPa. This rock-salt phase persists at high pressures, yielding a bulk modulus of 295 GPa. Phonon density of states and related thermal properties were measured by Nipko and Loong[6,7] by time-of flight neutron spectroscopy in a polycrystalline sample. They used a rigid-ion model to calculate the phonon dispersion, lattice specific heat, and Debye temperature. Inelastic x-ray scattering measurements were also reported by Schwoerer-Böhning *et al.*[8] to obtain the phonon dispersion along three high-symmetry directions. Mashino *et al.*[9] used shock compression up to 150 GPa to observe the phase transition and the equation of state. Anisotropic thermal expansion was measured by Iwaga *et al.*[10] by x-ray powder diffractometry in the temperature range of 300–1400 K. Raman-scattering, photoluminescence, and photoabsorption data have been reported by Senawiratne *et al.*[11] Elastic constants of AlN were measured using Brillouin spectroscopy by Kazan *et al.*,[12] who also reported the temperature dependence of Raman active modes in AlN.[13]

Theoretically, several *ab initio* calculations are found in the literature. First-principles molecular dynamics (MD) simulations of amorphous $Al_xGa_{1-x}N$ alloys were performed by Chen *et al.*[14] and Chen and Drabold.[15] The electronic structure of the wurtzite-phase AlN was investigated by means of the Hartree–Fock method by Ruiz *et al.*,[16] while Christensen and Gorczyca,[17,18] used density functional

a)Electronic mail: priyav@usc.edu.

theory (DFT) in the local density approximation to describe the structural phase transformation under pressure. Using lattice dynamics results from an adiabatic bond-charge model, Alshaikhi and Srivastava[19] calculated the specific heat of cubic and hexagonal phases of BN, AlN, GaN, and InN. Bungaro *et al.*[20] used a density functional perturbation theory to calculate the phonon dispersion and density of states for wurtzite AlN, GaN, and InN. A plane-wave pseudopotential method was used by Wright and Nelson[21] to describe structural properties of wurtzite and cubic AlN and InN. Pandey *et al.*[22] used all-electron DFT to describe the atomic structure and electronic properties of nonpolar surfaces of AlN. Car–Parrinello MD simulation was used to study amorphous BN, AlN, and $AlBN_2$ by McCulloch *et al.*[23]

In this work, we propose an effective interatomic potential for AlN, includes two-body and three-body interactions. Thermal, mechanical, structural, and dynamical properties of wurtzite-crystalline and amorphous phases are studied, including two-body and three-body structural correlations, vibrational density of states, and pressure-induced phase transformation are calculated. The paper is divided into five sections. Section II describes the proposed interatomic potential. In Sec. III, thermal, structural, mechanical, and dynamical properties of crystalline AlN are discussed, and the amorphous phase of AlN is analyzed in Sec. IV. Conclusions are drawn in Sec. V.

II. INTERACTION POTENTIAL FOR ALN

The interatomic potential energy of the system with two-body and three-body interactions can be written as

$$V = \sum_{i<j} V_{ij}^{(2)}(r_{ij}) + \sum_{i,j<k} V_{jik}^{(3)}(r_{ij}, r_{ik}). \tag{1}$$

The same functional form has been used successfully for SiO_2,[24–30] Si_3N_4,[31–34] SiC,[35–39] Al_2O_3,[40–42] CdSe,[43,44] GaAs,[45,46] GaAs/InAs,[47–50] and Si/Si_3N_4 systems.[51–53] The two-body term includes steric-size effects, Coulomb interactions, charge-induced dipole, and van der Waals interactions, and is given by

$$V_{ij}^{(2)}(r) = \frac{H_{ij}}{r^{\eta_{ij}}} + \frac{Z_i Z_j}{r} e^{-r/\lambda} - \frac{D_{ij}}{r^4} e^{-r/\xi} - \frac{W_{ij}}{r^6}. \tag{2}$$

In Eq. (2), H_{ij} is the strength of the steric repulsion, Z_i the effective charge in units of the electronic charge $|e|$, D_{ij} and W_{ij} are the strength of the charge–dipole and van der Waals attractions, respectively, η_{ij} are the exponents of the steric repulsion, and λ and ξ are the screening lengths for the Coulomb and charge–dipole interactions, respectively. Here, $r \equiv r_{ij} = |\vec{r}_i - \vec{r}_j|$ is the distance between the ith atom at position $\vec{r}_i$ and the jth atom at position $\vec{r}_j$.

The two-body interatomic potential is truncated at $r_{\mathrm{cut}} = 7.6$ Å and is shifted for $r \le r_{cut}$ in order to have the potential and its first derivative continuous at r_{cut}.[54,55] The shifted two-body part of the interatomic potential is given by

$$V_{ij}^{(2shifted)}(r) = \begin{cases} V_{ij}^{(2)}(r) - V_{ij}^{(2)}(r_c) - (r - r_c)(dV_{ij}^{(2)}(r)/dr)_{r=r_c} & r \le r_c \\ 0 & r > r_c \end{cases}. \tag{3}$$

The screening in the Coulomb and charge–dipole interactions is included in order to avoid costly calculation of long-range interactions. It has been shown that the inclusion of the screening has no noticeable difference in the structural and dynamical properties except for optical phonons in the long wavelength limit.[55]

The three-body interaction potential is given by a product of spatial and angular dependent factors in order to describe bond-bending and bond-stretching characteristics:[39,40]

$$V_{jik}^{(3)}(r_{ij}, r_{ik}) = R^{(3)}(r_{ij}, r_{ik}) P^{(3)}(\theta_{jik}), \tag{4}$$

where

$$R^{(3)}(r_{ij}, r_{ik}) = B_{jik} \exp\left(\frac{\gamma}{r_{ij} - r_0} + \frac{\gamma}{r_{ik} - r_0}\right) \Theta(r_0 - r_{ij}) \Theta(r_0 - r_{ik}), \tag{5}$$

$$P^{(3)}(\theta_{jik}) = \frac{(\cos\theta_{jik} - \cos\bar{\theta}_{jik})^2}{1 + C_{jik}(\cos\theta_{jik} - \cos\bar{\theta}_{jik})^2}. \tag{6}$$

Here, B_{jik} is the strength of the three-body interaction, θ_{jik} is the angle formed by $\vec{r}_{ij}$ and $\vec{r}_{ik}$, $\bar{\theta}_{jik}$ and C_{jik} are constants, and $\Theta(r_0 - r_{ij})$ is the step function.

Following previous studies using the same form of interatomic potential, the exponents η_{ij} are chosen to be 7, 9, and 7 for Al–Al, Al–N, and N–N interactions, respectively. The screening lengths are $\lambda = 5.0$ Å and $\xi = 3.75$ Å. The other parameters in the interaction potential are determined using experimental values for the lattice constant, cohesive energy, bulk modulus, and some of the elastic constants for AlN. Table I compares the experimental and calculated elastic constants using the above interaction potential. Kazan *et al.*[12] and McNeil *et al.*[56] independently reported the elastic constants of AlN determined by Brillouin scattering. McNeil *et al.*[56] provide a first order Raman analyses of AlN single crystal data, whereas Kazan *et al.*[12] discuss the temperature dependence of AlN Raman active modes. Tsubouchi *et al.*[57] measured the high-frequency and low dispersion surface

TABLE I. Comparison of cohesive energy, E/N, bulk modulus, B, and elastic constants, $C_{\alpha\beta}$, for AlN between MD model and experiments. [Calculated from the relation, $C_{66}=(C_{11}-C_{12})/2$.]

	$E_{cohesive}$ (eV/N)	B (GPa)	C_{11} (GPa)	C_{12} (GPa)	C_{13} (GPa)	C_{33} (GPa)	C_{44} (GPa)	C_{66} (GPa)
Expt.	−5.76	207.9[a]	394[d]	134[d]	95[d]	394[b]	121[d]	131
		185[c]	411[e]	149[e]	99[e]	402[d]	125[e]	130[d]
		211[e]	345[f]	125[f]	120[f]	389[e]	118[f]	
		237[e]				395[f]		
		202[f]						
MD	−5.7605	211.097	435.2	148.1	107.5	356	80.6	143.6

[a]Reference 2.
[b]Reference 4.
[c]Reference 3.
[d]Reference 12.
[e]Reference 56.
[f]Reference 57.

acoustic waves on AlN-Al_2O_3 and AlN-Si devices. Table II lists the parameters for AlN interatomic potential.

MD simulations are performed using the above interatomic potential for two system sizes: a system with 3360 atoms (1680 Al and 1680 N) and another with 11 520 atoms (5760 Al and 5760 N), both at experimental density. Periodic boundary conditions are imposed, and the equations of motion are integrated using the velocity VERLET algorithm with a time step of 1.5 fs. Starting with crystalline wurtzite AlN at nominal density of $\rho=3.263$ g/cc, the system is heated and compressed using a constant number of particles, pressure, and temperature (NPT) ensemble.

III. CRYSTALLINE ALN PHASE

In this section, we present thermal, structural, mechanical, phase transformation, and dynamical properties of wurtzite-crystalline AlN.

A. Energetic of crystalline structure

Our interatomic potential is used first to calculate the total energy per particle, E, as a function of the volume per particle, V, for wurtzite, zinc-blende, and rocksalt structure, as shown in Fig. 1. The dashed lines are fits using the Murnaghan equation[58] of state, $E(V)=(BV/B'(B'-1))[B'(1-V_0/V)+(V_0/V)^{B'}-1]+E(V_0)$, where B, B', and V_0 are fitting parameters. We find that the wurtzite structure, which has the minimum energy at the experimental density, is more stable than zinc-blende by 2.4 meV/particle. The common tangent between wurtzite and rock-salt structures indicates that the pressure for structural transformation is around 24 GPa. This value is consistent with the reported pressures of wurtzite-to-rocksalt transformation of 12.5 GPa,[17] 20 GPa,[5] 19.2 GPa,[9] 14–20 GPa.[3]

From the Murnaghan equation of states fit, the cohesive energy per atom is obtained as −5.76 eV, −5.759 eV, and −5.497 eV for wurtzite, zinc-blende, and rocksalt phases, respectively. The calculated bulk modulus, B, and its first derivative with respect to pressure, B', are 219.7 GPa and 6.2 for wurtzite, 220.2 GPa and 5.01 for zinc-blende, and 226.8 GPa and 8.0 for rocksalt structures. These results compare well with experimental values as shown in Table I and the measured Birch coefficient and their pressure derivative for rocksalt, $B=221\pm5$ GPa and $B'=4.8\pm1$.[3]

TABLE II. Parameters for two-body and three-body terms of the interaction potential used in the MD simulation of AlN.

		Z_i (e)	λ (Å)	ξ (Å)	r_c (Å)	e (C)
Two-body	Al	1.0708	5.0	3.75	7.60	1.602×10^{-19}
	N	−1.0708				

		η_{ij}	H_{ij} (eV Å$^{\eta}$)	D_{ij} (eV Å^4)	W_{ij} (eV Å^6)
Two-body	Al–Al	7	507.668 6	0	0
	Al–N	9	367.055 46	24.7978	34.583 65
	N–N	7	1038.163 34	49.5956	0

		B_{jik} (eV)	$\bar{\theta}_{jik}$ (deg)	C_{jik}	γ (Å)	r_0 (Å)
Three-body	Al–N–Al	2.1536	109.47	20	1.0	2.60
	N–Al–N	2.1536	109.47	20	1.0	2.60

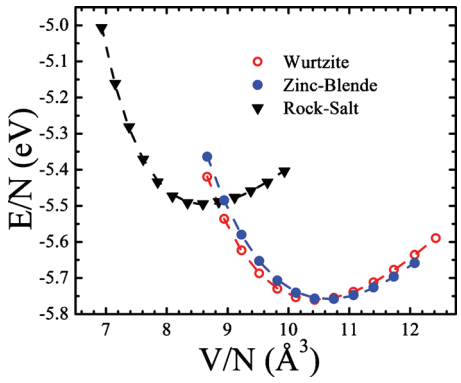

FIG. 1. (Color) Energy per particle as a function of the volume per particle for wurtzite, zinc-blende znd rock-slat structures. The difference in energy per particle between wurtzite and zinc-blende is 2.4 meV/N. The dashed lines are the fit form the Murnaghan equation of states.

In the Table I, lattice constant, cohesive energy, and bulk modulus are fitted to the experimental data, however, the elastic constants are not fitted and are derived from the interaction potential. Clearly, the agreement between our calculated results and experimental values for C_{11}, C_{12}, C_{13}, C_{33}, $[C_{66}=(C_{11}-C_{12})/2]$, is within 10% but the discrepancy between the calculated C_{44} values and experiment is about 40%. While the bulk modulus is determined mainly by the steric repulsion [first term in the Eq. (2)], the elastic constants are determined by both the two-body and three-body interaction terms. In a fourfold coordinated system like wurtzite, at equilibrium, the three-body potential, which has the form of a penalty function at the tetrahedral angle, contributes zero to the total energy. The three-body potential contributes to angular deformations from the ideal tetrahedral structure. For deformations where the bond length is unchanged but the bond-angles are distorted, three-body potential makes a contribution to the elastic constants. In spite of our considerable efforts, we are no able to clearly identify how a specific parameter in the interaction potential effects individual elastic constants. The reason for this is that the effect of a parameter has to be explored on the trajectory on which lattice constants, cohesive energy, and bulk modulus remain fixed, in agreement with experimental values. This implies that when a particular parameter is changed, say in three body part, the parameters in two-body potential have to be readjusted so that the lattice constants, cohesive energy, and bulk modulus remain at the experimental values. This procedure was explored with various parameters but no clear one-to-one relationship could be established between the parameters in the interaction potential and the individual elastic constants.

B. Melting of wurtzite AlN

Melting temperature is determined by increasing the temperature of crystalline phase (initially at 100 K) in steps of 100 K, where simulation is run for 3000 time steps using the NPT ensemble at each temperature. Figure 2 summarizes the total energy per atom and volume fraction, V/V_0, as a function of temperature (see the red circles). Here, V_0 is the volume of the system at 100 K. The system is found to melt

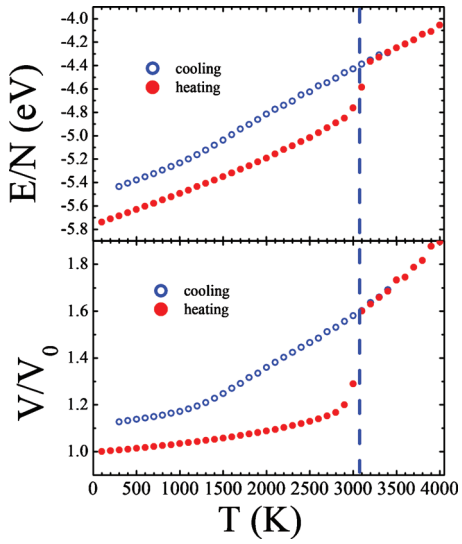

FIG. 2. (Color) Energy per particle and volume fraction, V/V_0, as a function of temperature. (V_0 is the volume of the system at 100 K). The vertical dashed line represents the calculated melting temperature of 3070 K.

at 3070 ± 50 K (see the vertical dashed line in Fig. 2). Experimentally, the melting temperature is reported to be 3273 (Ref. 59) or 3023 K (Ref. 60) between 100 and 500 atm of nitrogen pressure. Figure 2 also shows the energy per particle and the volume fraction during cooling from the liquid (the blue circles). An amorphous phase is thus obtained, and its structural and elastic properties will be discussed in Sec. IV.

Assuming a quadratic dependence on temperature, the volumetric thermal expansion coefficient for $100 < T < 1000$ is estimated as $\beta = 3.04 \times 10^{-5}$ K^{-1}, which is in reasonable agreement with the experimental value of $\beta = 1.3 \times 10^{-5}$ K^{-1}.[10]

C. Elastic properties of AlN

The elastic constants are calculated as a function of density (see the solid symbols in Fig. 3). The results show that C_{11} and C_{33} exhibit large density dependence. This is to be expected for as the density decreases and the interatomic distances increase, the strength of two-body and three-body interactions decrease, resulting in an overall decrease in the elastic constants and the bulk modulus. In the figure, open

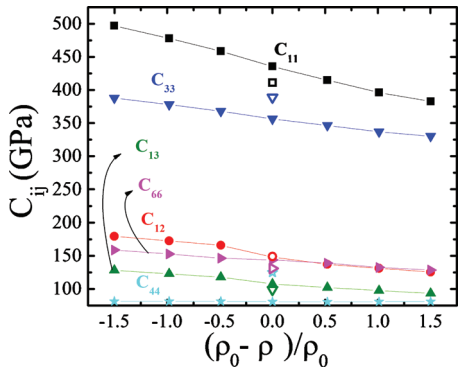

FIG. 3. (Color) Elastic constants as a function of density. Solid symbols are MD results, whereas open symbols are experimental values. ρ_0 is the initial density 3.263 g/cc.

TABLE III. Average values for elastic moduli calculated from MD at ρ =3.263 g/cc.

	⟨B⟩ (GPa)	⟨Y⟩ (GPa)	$\upsilon_{\parallel}$	$\upsilon_{\perp}$
Expt.	210[a]	310[b]	0.216[a]	0.287[a]
MD	217	334	0.184	0.287

[a]http://www.ioffe.ru/SVA/NSM/Semicond/AlN.
[b]http://www.anceram.de.

symbols are experimental values. It is notable that the MD results do not display any change in C_{44} as a function of density.

For a material with hexagonal symmetry, the elastic moduli, such as bulk modulus B, shear modulus G, Young modulus Y, and Poisson ratio ν, are crystallographic direction dependent, and are given by[61,62]

$$B = (C_{11}C_{33} + C_{12}C_{33} - 2C_{13}^2)/(2C_{33} + C_{11} - 4C_{13}),$$

$$Y_{\perp} = 2\left[\frac{C_{33}}{\Delta} + \frac{1}{C_{11} - C_{12}}\right]^{-1}, \quad Y_{\parallel} = \Delta/(C_{11} + C_{12}),$$

where $\Delta = C_{33}(C_{11}+C_{12}) - 2C_{13}^2$ and

$$\upsilon_{\parallel} = C_{13}/(C_{11} + C_{12}),$$

$$\upsilon_{\perp} = (C_{12}C_{33} - C_{13}^2)/(C_{11}C_{33} - C_{13}^2),$$

where the parallel and perpendicular symbols are for the directions out of and in the basal plane, respectively. The average elastic moduli of a hexagonal crystal is given by

$$\langle B \rangle = \frac{2}{9}(C_{11} + C_{12} + 2C_{13} + C_{33}/2),$$

$$\langle Y \rangle = (2Y_{\perp} + Y_{\parallel})/3.$$

MD results for these quantities are summarized in Table III.

Densification influences the mechanical properties of material. Figure 4 shows an MD prediction of elastic moduli as a function of density.

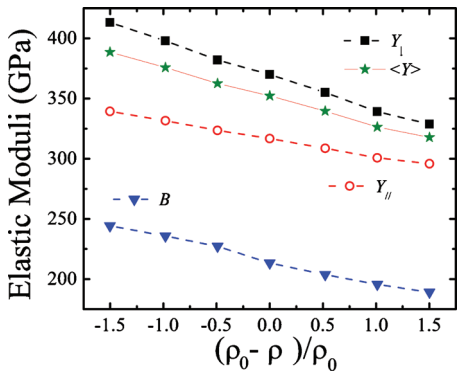

FIG. 4. (Color) Young modulus and bulk modulus calculated for crystalline AlN phase as a function of density. Due to crystallographic dependence, the average Young modulus is also displayed.

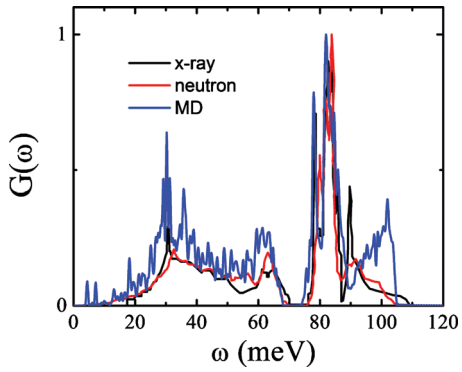

FIG. 5. (Color) Vibrational density of states. MD results are compared with experimental data from inelastic x-ray scattering and time of flight neutron spectroscopy.

D. Vibrational density of states of AlN

From the Fourier transform of the velocity-velocity autocorrelation function, we obtain the partial vibrational density of states,

$$G_{\alpha}(\omega) = \frac{6N_{\alpha}}{\pi}\int_0^{\infty} Z_{\alpha}(t)\cos(\omega t)dt, \tag{7}$$

where N_{α} is the number of atoms of species α (=Al or N),

$$Z_{\alpha}(t) = \frac{\langle \vec{v}_i(t)\cdot\vec{v}_i(0)\rangle_{i\in\alpha}}{\langle \vec{v}_i(0)\cdot\vec{v}_i(0)\rangle_{i\in\alpha}} \tag{8}$$

is the velocity-velocity autocorrelation function, $\vec{v}_i(t)$ is the velocity of the ith atom at time t, and the brackets denote averages over ensembles and atoms of species α, and the total density of states $G(\omega)$ is defined as

$$G(\omega) = \sum_{\alpha} G_{\alpha}(\omega). \tag{9}$$

Figure 5 shows the calculated vibrational density of states along with experimental phonon densities of states reported by Nipko and Loong[6,8] using neutron time of flight measurement and by Schwoerer-Böhning *et al.*[8] using inelastic x-ray scattering.

From partial density of states (Fig. 6) we can identify that the main contribution to the low frequency spectra

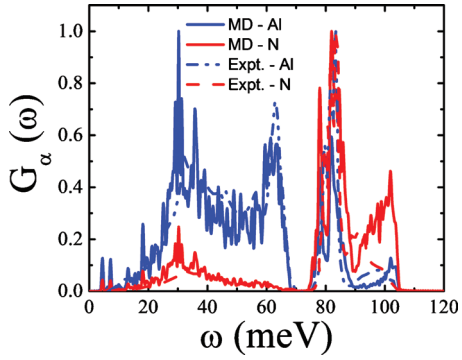

FIG. 6. (Color) Partial vibrational density of states calculated by Eq. (7) are compared with experimental data by Nipko and Loog (Refs. 6 and 8) using neutron time of flight spectroscopy.

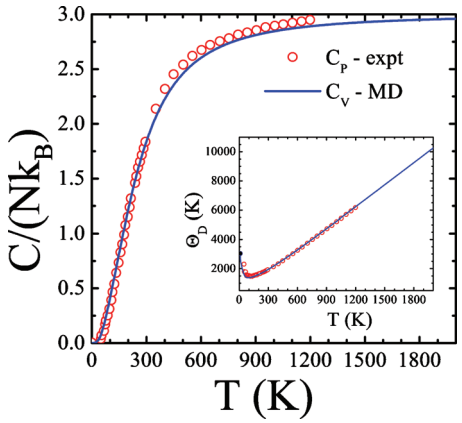

FIG. 7. (Color) Calculated heat capacity at constant volume, C_V and experimental C_P as a function of temperature for wurtzite AlN. The inset depicted the Debye temperature calculated from the low temperature expression $C_V = (12/5)\pi^4 N k_B (T/\Theta_D)^3$.

comes from Al vibrations, in particular the 30 and 60 meV are the most intense peaks coming from Al. The optical modes are due to both vibrations.

E. Specific heat of crystalline AlN

The lattice heat capacity at constant volume is calculated from the vibrational density of states as a function of temperature. Figure 7 shows the calculated C_V/Nk_B along experimental values of C_P reported by Koshchenko *et al.*[1] The agreement is good over the entire range of temperature. At low temperatures, the Debye temperature, Θ_D, can be obtained through $C_V=(12/5)\pi^4 N k_B (T/\Theta_D)^3$, and the result is revealed in the inset of Fig. 7. Using the experimental specific heat[1] and the same expression, the "experimental" Debye temperature is also plotted in the inset. The agreement between MD and experimental Θ_D is excellent for all temperature range up to 2000 K.

F. Pressure-induced phase transformation

The common tangent of the energy versus atomic volume between wurtzite and rock-salt structures shown in Fig. 1 correctly predicts the pressure of transformation. The transformation pressure is also obtained dynamically using MD simulations by increasing the external pressure at constant temperature. Starting at zero pressure, the system is first heated to 3000 K, before melting. Keeping the temperature constant at this value, two sets of simulations are performed. First, the pressure is increased in steps of 0.5 GPa, and simulation is run for 1000 time steps at each pressure, until the final pressure of 60 GPa. In the second set of simulations, the pressure is decreased using the same schedule. Figure 8 shows the volume versus pressure for AlN for both upstroke (solid circles) and downstroke (open triangles). V_0 is the initial volume at zero pressure. The phase transformation starts at around 27.5 GPa and is completed at 29 GPa. The decrease in volume during the transformation $(V_I - V_{II})/V_I$ (where V_I and V_{II} are the volume per atom just before and after the phase transition, respectively) is calculated to be 14%. This is slightly different from the value, 18.6%, reported by Xia *et al.*[3] The difference is related to the different

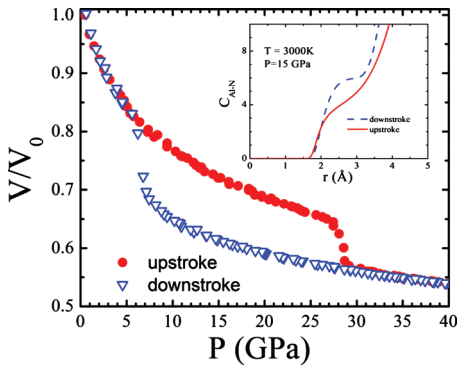

FIG. 8. (Color) Volume fraction V/V_0 as a function of temperature. V_0 is the volume of the system at zero pressure and 100 K. Solid circles are for hydrostatic compression and open triangles are for decompression. The coordination number at 15 GPa, for compression and decompression in the inset shows that the phase transformation has occurred.

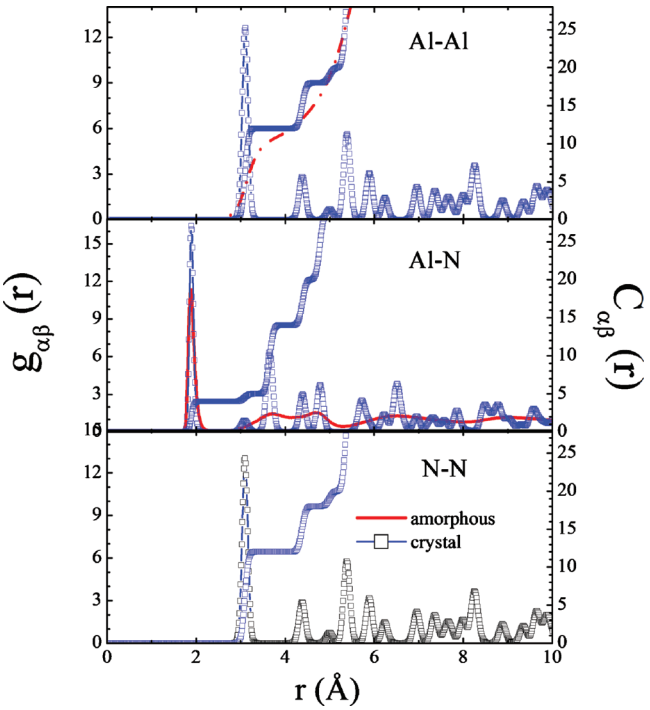

FIG. 9. (Color) Partial pair distribution function for crystalline and amorphous AlN. The amorphous phase has density of 2.966 g/cc.

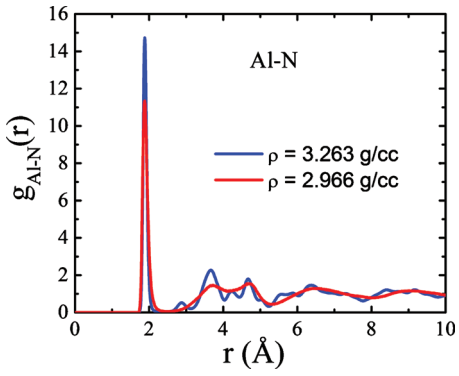

FIG. 10. (Color) Al–N pair distribution function for amorphous AlN at two densities.

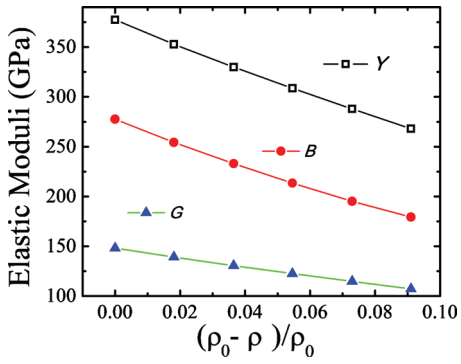

FIG. 11. (Color) Elastic moduli of amorphous AlN as a function of density. ρ_0 is the density of the crystalline phase (ρ_0=3.262 g/cc).

conditions: In our simulation, the temperature is fixed at 3000 K, whereas experimentally it was 300 K. This is done primarily to expedite the transformation within a reasonable simulation time. The inset in Fig. 8 display the Al–N coordination number. At same pressure and temperature in upstroke regime the Al atoms are coordinated by four N atoms, while in downstroke the coordination is six, characteristic of the rock-salt structure.

IV. AMORPHOUS ALN

Amorphous AlN is obtained by cooling from the liquid. Starting from a liquid at 3500 K, the temperature is decreased in steps of 100 K, where simulation is run for 3000 time steps at each temperature, in order to obtain an amorphous system at 300 K. At this temperature, the system is thermalized for 20 000 time steps before computing average quantities. Amorphous systems at two densities are obtained: one at the crystal density, and the other with 10% smaller density. As shown in Fig. 2, fast cooling results in an amorphous phase with about 10% larger volume.

A. Structural correlations for amorphous AlN

Calculated partial pair distribution functions, $g_{\alpha\beta}(r)$, and corresponding coordination numbers, $C_{\alpha\beta}(r)$,[30] at 300 K for amorphous AlN, are shown in Fig. 9, along with the crystalline results at the same temperature. The elemental tetrahedral unit is preserved in the amorphous state.

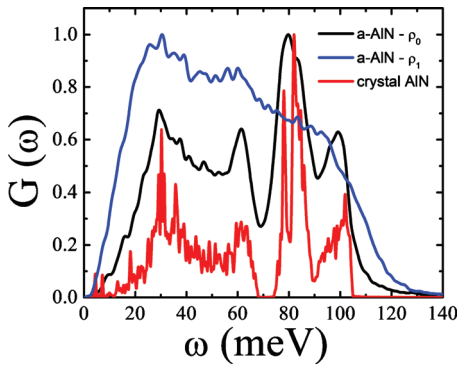

FIG. 12. (Color) Calculated vibrational density of states for amorphous a-AlN at T=300 K. ρ_0 is the density of the crystalline phase (ρ_0 =3.262 g/cc) and ρ_1=2.966 g/cc. The result for the crystalline is also shown for comparison.

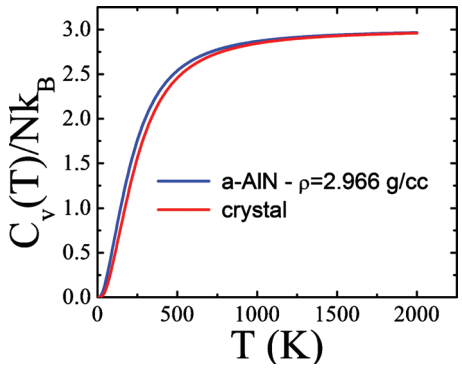

FIG. 13. (Color) Constant volume heat capacity calculated from MD vibrational density of states for amorphous AlN. Result for wurtzite AlN at 3.263 g/cc is also shown.

At higher density, the amorphous state is more structured, as shown in Fig. 10. This is reflected in the vibrational density of states, as discussed in Sec. IV C.

B. Elastic moduli of amorphous AlN

The elastic moduli for amorphous phase are computed (see Fig. 11) as a function of density assuming that the system is isotropic. Young modulus is then given by $Y=(C_{11}-C_{12})(C_{11}+2C_{12})/(C_{11}+C_{12})$, Poisson ratio by $\nu=C_{12}/(C_{11}+C_{12})$, bulk modulus by $B=Y/[3(1-2\nu)]$, and shear modulus by $G=Y/[2(1+\nu)]$. Poisson ratio is practically independent of density, varying from 0.274 (density ρ=3.263 g/cc of wurtzite crystal) to 0.251 (ρ=2.966 g/cc).

C. Dynamical properties of amorphous AlN

The vibrational density of states at 300K for amorphous AlN is shown in Fig. 12. We observe that the densification of the amorphous phase mentioned in Sec. IV A results in vibrational modes that resemble those of the crystalline material.

Figure 13 shows the calculated heat capacity at constant volume, C_v, for amorphous phase. We see that C_v of amorphous phase is slightly larger than the crystalline heat capacity. This is due to the increased number of low-frequency vibrational modes, as is shown in Fig. 12. When the density of the amorphous phase is the same as the crystal density, the heat capacity is essentially the same as the crystalline phase.

V. CONCLUSIONS

We have developed an effective interatomic potential for AlN consisting of two-body and three-body terms for MD simulations. The proposed interaction potential correctly describes cohesive energy, bulk modulus, elastic constants, and melting temperature of wurtzite crystal. The MD vibrational density of states also compares favorably with the neutron experiments. The specific heat also compares well with the experiments. The interaction potential has been used for MD simulation study of pressure-induced structural phase transformation. Predictions are made for the elastic constants for crystalline and amorphous states at different densities and amorphous phase at different densities.

ACKNOWLEDGMENTS

This work was partially supported by the Theory Program of the Materials Sciences and Engineering Division and the Center for Energy Nanoscience, an Energy Frontier Research Center, of the DOE-Office of Basic Energy Sciences, the SciDAC program of the DOE-Office of Advanced Computing Research, NSF-PetaApps, and NSF-EMT. J.P.R. acknowledges financial support from Brazilian agencies Fundação de Amparo à Pesquisa do Estado de São Paulo (FAPESP) and Conselho Nacional de Desenvolvimento Científico e Tecnológico (CNPq).

[1]V. I. Koshchenko, Y. K. Grinberg, and A. F. Demidenko, Inorg. Mater. **20**, 1550 (1984).
[2]M. Ueno, A. Onodera, O. Shimomura, and K. Takemura, Phys. Rev. B **45**, 10123 (1992).
[3]Q. Xia, H. Xia, and A. L. Ruoff, J. Appl. Phys. **73**, 8198 (1993).
[4]W. J. Meng, J. A. Sell, T. A. Perry, and G. L. Eesley, J. Vac. Sci. Technol. A **11**, 1377 (1993).
[5]S. Uehara, T. Masamoto, A. Onodera, M. Ueno, O. Shimomura, and K. Takemura, J. Phys. Chem. Solids **58**, 2093 (1997).
[6]J. C. Nipko and C.-K. Loong, Phys. Rev. B **57**, 10550 (1998).
[7]J. C. Nipko, C. K. Loong, C. M. Balkas, and R. F. Davis, Appl. Phys. Lett. **73**, 34 (1998).
[8]M. Schwoerer-Böhning, A. T. Macrander, M. Pabst, and P. Pavone, Phys. Status Solidi B **215**, 177 (1999).
[9]T. Mashimo, M. Uchino, A. Nakamura, T. Kobayashi, E. Takasawa, T. Sekine, Y. Noguchi, H. Hikosaka, K. Fukuoka, and Y. Syono, J. Appl. Phys. **86**, 6710 (1999).
[10]H. Iwanaga, A. Kunishige, and S. Takeuchi, J. Mater. Sci. **35**, 2451 (2000).
[11]J. Senawiratne, M. Strassburg, N. Dietz, U. Haboeck, A. Hoffmann, V. Noveski, R. Dalmau, R. Schlesser, and Z. Sitar, Phys. Status Solidi C **2**, 2774 (2005).
[12]K. Kazan, E. Moussaed, R. Nader, and P. Masri, Phys. Status Solidi C **4**, 204 (2007).
[13]M. Kazan, C. Zgheib, E. Moussaed, and P. Masri, Diamond Relat. Mater. **15**, 1169 (2006).
[14]H. Chen, K. Y. Chen, D. A. Drabold, and M. E. Kordesch, Appl. Phys. Lett. **77**, 1117 (2000).
[15]K. Y. Chen and D. A. Drabold, J. Appl. Phys. **91**, 9743 (2002).
[16]E. Ruiz, S. Alvarez, and P. Alemany, Phys. Rev. B **49**, 7115 (1994).
[17]N. E. Christensen and I. Gorczyca, Phys. Rev. B **47**, 4307 (1993).
[18]N. E. Christensen and I. Gorczyca, Phys. Rev. B **50**, 4397 (1994).
[19]A. AlShaikhi and G. P. Srivastava, Phys. Status Solidi C **3**, 1495 (2006).
[20]C. Bungaro, K. Rapcewicz, and J. Bernholc, Phys. Rev. B **61**, 6720 (2000).
[21]A. F. Wright and J. S. Nelson, Phys. Rev. B **51**, 7866 (1995).
[22]R. Pandey, P. Zapol, and M. Causa, Phys. Rev. B **55**, R16009 (1997).
[23]D. G. McCulloch, D. R. McKenzie, and C. M. Goringe, J. Appl. Phys. **88**, 5028 (2000).
[24]T. J. Campbell, R. K. Kalia, A. Nakano, F. Shimojo, K. Tsuruta, P. Vashishta, and S. Ogata, Phys. Rev. Lett. **82**, 4018 (1999).
[25]Y. C. Chen, Z. Lu, K. I. Nomura, W. Wang, R. K. Kalia, A. Nakano, and P. Vashishta, Phys. Rev. Lett. **99**, 155506 (2007).
[26]Y. C. Chen, K. Nomura, R. K. Kalia, A. Nakano, and P. Vashishta, Phys. Rev. Lett. **103**, 035501 (2009).
[27]Z. Lu, K. Nomura, A. Sharma, W. Q. Wang, C. Zhang, A. Nakano, R. Kalia, P. Vashishta, E. Bouchaud, and C. Rountree, Phys. Rev. Lett. **95**, 135501 (2005).
[28]A. Nakano, L. S. Bi, R. K. Kalia, and P. Vashishta, Phys. Rev. Lett. **71**, 85 (1993).
[29]A. Nakano, R. K. Kalia, and P. Vashishta, Phys. Rev. Lett. **73**, 2336 (1994).
[30]P. Vashishta, R. K. Kalia, J. P. Rino, and I. Ebbsjo, Phys. Rev. B **41**, 12197 (1990).
[31]R. K. Kalia, A. Nakano, A. Omeltchenko, K. Tsuruta, and P. Vashishta, Phys. Rev. Lett. **78**, 2144 (1997).
[32]R. K. Kalia, A. Nakano, K. Tsuruta, and P. Vashishta, Phys. Rev. Lett. **78**, 689 (1997).
[33]A. Nakano, R. K. Kalia, and P. Vashishta, Phys. Rev. Lett. **75**, 3138 (1995).
[34]P. Vashishta, R. K. Kalia, and I. Ebbsjo, Phys. Rev. Lett. **75**, 858 (1995).
[35]A. Chatterjee, R. K. Kalia, A. Nakano, A. Omeltchenko, K. Tsuruta, P. Vashishta, C. K. Loong, M. Winterer, and S. Klein, Appl. Phys. Lett. **77**, 1132 (2000).
[36]H. P. Chen, R. K. Kalia, A. Nakano, P. Vashishta, and I. Szlufarska, J. Appl. Phys. **102**, 063514 (2007).
[37]F. Shimojo, I. Ebbsjo, R. K. Kalia, A. Nakano, J. P. Rino, and P. Vashishta, Phys. Rev. Lett. **84**, 3338 (2000).
[38]I. Szlufarska, A. Nakano, and P. Vashishta, Science **309**, 911 (2005).
[39]P. Vashishta, R. K. Kalia, A. Nakano, and J. P. Rino, J. Appl. Phys. **101**, 103515 (2007).
[40]P. Vashishta, R. K. Kalia, A. Nakano, and J. P. Rino, J. Appl. Phys. **103**, 083504 (2008).
[41]C. Zhang, R. K. Kalia, A. Nakano, and P. Vashishta, Appl. Phys. Lett. **91**, 071906 (2007).
[42]C. Zhang, R. K. Kalia, A. Nakano, and P. Vashishta, Appl. Phys. Lett. **91**, 121911 (2007).
[43]N. J. Lee, R. K. Kalia, A. Nakano, and P. Vashishta, Appl. Phys. Lett. **89**, 093101 (2006).
[44]F. Shimojo, S. Kodiyalam, I. Ebbsjo, R. K. Kalia, A. Nakano, and P. Vashishta, Phys. Rev. B **70**, 184111 (2004).
[45]S. Kodiyalam, R. K. Kalia, H. Kikuchi, A. Nakano, F. Shimojo, and P. Vashishta, Phys. Rev. Lett. **86**, 55 (2001).
[46]S. Kodiyalam, R. K. Kalia, A. Nakano, and P. Vashishta, Phys. Rev. Lett. **93**, 203401 (2004).
[47]P. S. Branicio, R. K. Kalia, A. Nakano, J. P. Rino, F. Shimojo, and P. Vashishta, Appl. Phys. Lett. **82**, 1057 (2003).
[48]P. S. Branicio, J. P. Rino, F. Shimojo, R. K. Kalia, A. Nakano, and P. Vashishta, J. Appl. Phys. **94**, 3840 (2003).
[49]X. T. Su, R. K. Kalia, A. Nakano, P. Vashishta, and A. Madhukar, Appl. Phys. Lett. **79**, 4577 (2001).
[50]X. T. Su, R. K. Kalia, A. Nakano, P. Vashishta, and A. Madhukar, Appl. Phys. Lett. **78**, 3717 (2001).
[51]M. E. Bachlechner, A. Omeltchenko, A. Nakano, R. K. Kalia, P. Vashishta, I. Ebbsjo, and A. Madhukar, Phys. Rev. Lett. **84**, 322 (2000).
[52]E. Lidorikis, M. E. Bachlechner, R. K. Kalia, A. Nakano, P. Vashishta, and G. Z. Voyiadjis, Phys. Rev. Lett. **87**, 086104 (2001).
[53]A. Omeltchenko, M. E. Bachlechner, A. Nakano, R. K. Kalia, P. Vashishta, I. Ebbsjo, A. Madhukar, and P. Messina, Phys. Rev. Lett. **84**, 318 (2000).
[54]M. P. Allen and D. J. Tildesley, *Computer Simulation of Liquids* (Clarendon, Oxford, 1987).
[55]A. Nakano, R. K. Kalia, and P. Vashishta, J. Non-Cryst. Solids **171**, 157 (1994).
[56]L. E. McNeil, M. Grimsditch, and R. H. French, J. Am. Ceram. Soc. **76**, 1132 (1993).
[57]K. Tsubouchi, K. Sugai, and N. Mikoshiba, *Ultrasonics Symposia Proceedings* (IEEE, New York, 1981), p. 375.
[58]F. D. Murnaghan, Proc. Natl. Acad. Sci. U.S.A. **30**, 244 (1944).
[59]J. B. MacChesney, P. M. Bridenbaugh, and P. B. O'Connor, Mater. Res. Bull. **5**, 783 (1970).
[60]Y. Goldberg, *Properties of Advanced Semiconductor Materials: GaN, AlN, InN, BN, SiC, SiGe* (Wiley, New York, 2001), Vol. XVII, p. 194.
[61]V. T. Golovchan, Int. Appl. Mech. **34**, 755 (1998).
[62]L. D. Landau and E. M. Lifshitz, *Theory of Elasticity* (Pergamon, Oxford, 1970), Vol. 7.